

# Ratchet transport and periodic structures in parameter space

A. Celestino<sup>1</sup>, C. Manchein<sup>2</sup>, H.A. Albuquerque<sup>1</sup> and M.W. Beims<sup>2</sup>

<sup>1</sup>*Departamento de Física, Universidade do Estado de Santa Catarina, 89219-710 Joinville, SC, Brazil and*

<sup>2</sup>*Departamento de Física, Universidade Federal do Paraná, 81531-980 Curitiba, PR, Brazil*

(Dated: April 1, 2019)

Ratchet models are prominent candidates to describe the transport phenomenon in nature in the absence of external bias. This work analyzes the parameter space of a discrete ratchet model and gives direct connections between chaotic domains and a family of *isoperiodic stable structures* with the ratchet current. The isoperiodic structures appear along preferred direction in the parameter space giving a guide to follow the current, which usually increases inside the structures but is independent of the corresponding period. One of such structures has the shrimp-shaped form which is known to be an universal structure in the parameter space of dissipative systems. Currents in parameter space provide a direct measure of the momentum asymmetry of the multistable and chaotic attractors *times* the size of the corresponding basin of attraction. Transport structures are shown to exist in the parameter space of the Langevin equation with an external oscillating force.

PACS numbers: 05.45.Ac, 05.45.Pq

Keywords: Shrimps, ratchet currents, transport.

The description of the ratchet transport of particles in nature has become an actual and large studied problem due to the possibility to obtain transport properties without external bias. To obtain ratchet transport, spatiotemporal symmetries must be broken in the system [1]. Ratchets have become natural candidates to describe transport phenomena in Brownian [2, 3] and molecular motors [4], cold atoms [5], migration of bacteria [6], cell mobility in cancer metastasis [7], granular gas [8], fluid transport [9] and in more general areas like classical and quantum physics [10], chemistry [11, 12] and biophysics [13]. These are just some references in the distinct areas, since the actual literature related to ratchets is enormous.

A common feature of interest in all areas of ratchets applications is the understanding, achievement and control of transport. A priori, dynamical variables and parameters of the system (like temperature, dissipation, noise intensity, external forces etc.), which control the dynamics, are deeply interconnected so that it is very hard to make general statements about the ratchet current ( $\mathcal{RC}$ ) as a function of the parameters. The precise determination of the nature of transport in unbounded systems is still not fully understood, thus it is very desirable to achieve and/or recognize “patterns” or “structures” in the parameter space which are directly connected to transport properties. Even more attractive if such transport structures present universal features observed in a large class of dynamical systems.

This Letter analyzes the parameter space of a ratchet model and shows the relation between ratchet currents with a family of *isoperiodic stable structures* (ISSs) and *chaotic domains* in parameter space. In this way a remarkable complete connection between parameters of the system and the  $\mathcal{RC}$  is given, and therefore general clues for the origin of directed transport. To mention an example, one of the ISSs observed here, which has the shrimp-shaped form [see Fig. 3(c)], has already appeared

in the parameter space of generic dynamical systems and applications. Such shrimps were found to be universal structures in the parameter space of dissipative systems like maps [14–16] and continuous models [17], among others. Very recently they were also observed in experiments with electronic circuits [18]. We show here that such shrimp-shaped structures are also essential concerning directed transport in nature and we stress that this is valid for any ratchet model and applications.

In order to show generic properties of the  $\mathcal{RC}$  in the parameter space, we use a Map which presents all essential features regarding unbiased current [19]

$$M : \begin{cases} p_{n+1} = \gamma p_n + K[\sin(x_n) + a \sin(2x_n + \phi)], \\ x_{n+1} = x_n + p_{n+1}, \end{cases} \quad (1)$$

where  $p_n$  is the momentum variable conjugated to  $x_n$ ,  $n = 1, 2, \dots, N$  represents the discrete time and  $K$  is the nonlinearity parameter. The dissipation parameter  $\gamma$  reaches the overdamping limit for  $\gamma = 0$  and the conservative limit for  $\gamma = 1$ . The ratchet effect appears due to the spatial asymmetry, which occurs with  $a \neq 0$  and  $\phi \neq m\pi$  ( $m = 1, 2, \dots$ ), in addition to the time reversal asymmetry for  $\gamma \neq 1$ . The  $\mathcal{RC}$  of the above model was studied [19] for fixed  $K = 6.5$  in the dissipation interval  $0 \leq \gamma < 1$ . It was shown that close to the limit  $\gamma = 1$  the  $\mathcal{RC}$  arises due to the mixture of chaotic motion with tiny island (accelerator modes) from the conservative case, while for smaller values of  $\gamma$ , chaotic and stable periodic motion generates the current.

Figure 1 shows the  $\mathcal{RC}$  (colors) as a function of the dissipation parameter  $\gamma$  and the nonlinearity parameter  $K$ . A remarkable complex structure of colors is evident, where each color is related to a given value of the current (see color bar). Black colors are related to close to zero currents; green, blue to purple colors are related to increasing positive currents while red, yellow to white

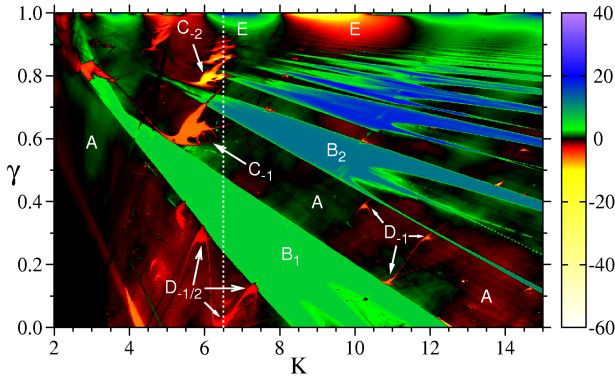


Figure 1. (Color online) The current (see color bar) plotted in the parameter space  $(K, \gamma)$  with a grid of  $600 \times 600$  points,  $a = 0.5$ ,  $\phi = \pi/2$ ,  $10^5$  initial conditions with  $\langle p_0 \rangle = \langle x_0 \rangle = 0$  inside the unit cell  $(-2\pi, 2\pi)$ , and  $N = 10^4$  iterations.

colors related to increasing negative currents. The white straight line at  $K = 6.5$  corresponds to the case analyzed recently [19]. Three main regions with distinct behaviors can be identified: (i) a large “cloudy” background, identified as A in Fig. 1, mixed with black, red and green colors, showing a mixture of zero, small negative and positive currents, respectively; (ii) several structures with sharp borders and distinct colors, which are embedded in the cloudy background region and are identified in Fig. 1 as  $B_L, C_L$  and  $D_L$  ( $L$  is an integer or rational number); (iii) strong positive and negative currents (region E), with not well defined borders which occur close to the conservative limit  $\gamma = 1$ . At next we explain in more details these distinct regions by analyzing other quantities.

Figure 2 shows the parameter space  $(K, \gamma)$  for the period- $q$  from the orbits. Periodic stable motion is restricted to well defined structures while the black background is related to the chaotic motion. This was checked by determining (not shown) the parameter space for the largest Lyapunov exponent (LE). Zero and negative LEs are related to the periodic motion and positive LEs to the black regions of Fig. 2. This already allow us to associate the cloudy region A from Fig. 1 with the chaotic motion. Thus the small portions of negative/positive currents (red and green clouds) are due to the chaotic transport, consequence of the asymmetry of the chaotic attractor [5].

Map (1) is periodic in  $x$  with period  $2\pi$ . Thus the condition for a period- $q$  orbit is  $\sum_{i=n}^{n+q-1} p_i = 2\pi m$ , with integer  $m = \dots, -2, -1, 0, 1, 2, \dots$  which represent the net number of left (negative) or right (positive)  $2\pi$  jumps in  $x$  over the period. The mean momentum for a given period- $q$  is then  $\bar{p}_q = \sum_{i=n}^{n+q-1} p_i / q = 2\pi m / q$  which can be written as  $2\pi L$ , so that  $L = m / q$ . Therefore  $L$ , which gives  $\bar{p}_q$  in units of  $2\pi$ , can assume fractional values (positive or negative). All sharp borders from  $B_L, C_L$  and  $D_L$  in Fig. 1 coincide with those of Fig. 2 and a direct con-

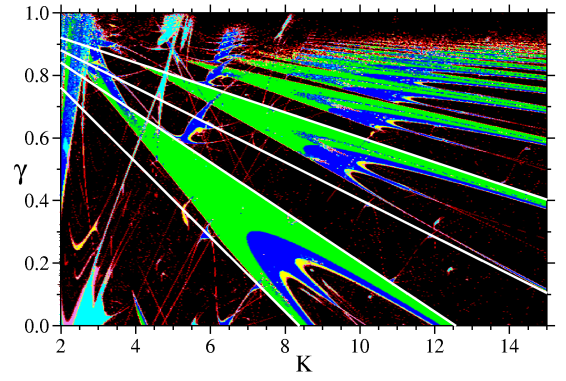


Figure 2. (Color online) Period- $q$  values in parameter space  $(K, \gamma)$ : green:  $q = 1$ , blue:  $q = 2$ , cyan:  $q = 3$ , yellow:  $q = 4$ , pink:  $q = 6$ , red  $q \geq 8$  and black for no period. In this case only one initial condition is used ( $x_0 = 0.5, p_0 = 0.3$ ),  $N = 10^6$  iterations and a grid of  $600 \times 600$  points.

nection between periodic stable motion and the  $\mathcal{RC}$  is given. Regarding these sharp structures we observe three different ISSs:  $B_L$  composed by the sequence  $L = 1, 2, \dots$  of dominant diagonal structures with main period  $q = 1$  (see green main regions in Fig. 2) which extend themselves along a large range of  $K$  values. As  $K$  increases and  $\gamma$  decreases, inside each structure  $B_L$  we observe  $1 \times 2^n$  (green  $\rightarrow$  blue  $\rightarrow$  yellow  $\rightarrow \dots$ ) and  $3 \times 2^n$  (cyan  $\rightarrow$  pink  $\rightarrow \dots$ ) doubling cascades bifurcations. Comparing to Fig. 1, we observe that the current inside each structure  $B_L$  is independent of the period  $q$  and thus, on the bifurcation points. At the doubling bifurcation cascades  $1 \times 2^n$  we observed that  $m \rightarrow 2m$  so that  $L (= m/q = \bar{p}_q/2\pi)$  remains constant inside each structure  $B_L$ . On the other hand, even though different isoperiodic  $B_L$  structures have the same period,  $\mathcal{RC}$ s increase with  $L$ , as can be seen in Fig. 1 when  $\gamma$  and  $L$  increase. Structures  $B_L$  are very similar to the cuspidal singularities [20]. Since the boundary of the dominant structures  $B_L$  are born at period  $q = 1$ , these borders can be calculated analytically from the eigenvalues of the Jacobian of the map (1) after one iteration. Using  $\phi = \pi/2$ , the fixed points from (1) can be calculated from  $p^{(1)} = 2\pi L$  ( $L$  integer) and  $2\pi L(\gamma - 1) + K [\sin(x^{(1)}) + a \cos(2x^{(1)})] = 0$ . The solutions are  $x_j^{(1)} = \arctan(\alpha^{(-)}, \pm \beta^{(+)})$  ( $j = 1, 2$ ) and  $x_s^{(1)} = \arctan(\alpha^{(+)}, \pm \beta^{(-)})$  ( $s = 3, 4$ ) where  $\alpha^{(\mp)} = \mp \sqrt{K [3K + 8L\pi(\gamma - 1)]} + K$  and  $\beta^{(\pm)} = \sqrt{8KL\pi(1 - \gamma) \pm 2\sqrt{K^2 [3K + 8L\pi(\gamma - 1)]}}$ . Substituting these solutions in the Jacobian of the map (1) we obtain analytical expressions  $\lambda(\gamma, K, L)$  for the two eigenvalues. When  $\lambda(\gamma, K, L) = +1$  (born of period-1), we obtain a relation between  $\gamma, K$  and  $L$  where period-1 orbits are born in parameter space. The solutions for  $\lambda(\gamma, K, L) - 1 = 0$ , for all fixed points  $x_j^{(1)}$ , are  $\gamma_1^{(L)} = 1 - 3K/(8\pi L)$  (lower border) and  $\gamma_2^{(L)} = 1 - K/(4\pi L)$

(upper border). Both curves define exactly, for a given  $L$ , the sharp period-1  $B_L$  boundaries of Figs. 1 and 2. The border of the first large dominant structure  $B_1$  is obtained from  $L = 1$ , the second one  $B_2$  from  $L = 2$ , and so on. See white lines  $\gamma_1^{(L=1)}$ ,  $\gamma_2^{(L=1)}$ ,  $\gamma_1^{(L=2)}$ , and  $\gamma_2^{(L=2)}$  in Fig. 2. Looking carefully however, all (for any  $L$ ) lower borders  $\gamma_2^{(L)}$  do not match exactly with the simulations. For these regions the basin of attraction from the chaotic attractor is much larger compared to the basin of attraction related to the fixed point, and thus the current related to period 1 is too small and is not observed. This is also exactly what is observed in Fig. 3 from [19], where the left limits of the  $L$  intervals are inside the chaotic region. As  $L$  increases,  $\gamma_1^{(L \rightarrow \infty)} \rightarrow \gamma_2^{(L \rightarrow \infty)} \rightarrow 1$  and the dominant structures approach to each other more and more.

The second kind of relevant ISSs,  $C_L$ , can be visualized in Fig. 1 close to  $K = 6.0$  and  $\gamma > 0.6$ . They also are ordered in a sequence of structures  $L = -1, -2, \dots$  which approach each other as  $\gamma$  increases, defining a direction in the parameter space obtained by the straight line  $\gamma = 0.2845K - 0.994925$ , along which negative currents increase [see dashed line in Fig. 3(a)]. The main period of each  $C_L$  is  $q = 2$  (blue) [Fig. 3(b)] but, inside each structure,  $1 \times 2^n$  (blue  $\rightarrow$  yellow  $\rightarrow$  red  $\rightarrow \dots$ ) doubling cascades bifurcations appears when going to the border of the structures, where the chaotic region is reached. For clarification Figs. 3(a)-(b) present the current and period as a magnification for these structures. Again we observe that current increases (in modulus) along the sequences as  $\gamma$  increases.

The last observed ISSs,  $D_L$ , appear embedded in the cloudy chaotic background and present the well known shrimp-shaped form. For example, three connected structures ( $D_{-1}$ ) appear in red in the interval  $10 < K < 12$  and  $0.1 < \gamma < 0.4$  [see also Fig. 3(c)]. Another example of shrimp-shaped structures is demarked in Fig. 1 by  $D_{-1/2}$ . These structures have a main body with period  $q = 2$  and a succession of domains related to period-doubling route to chaos. Shrimps-shaped structures are also distributed in sequences along preferred direction in the parameter space, as can be seen by looking carefully to Fig. 1, where many shrimp-shaped structures are hidden behind the dominant  $B_L$  structures. Such preferential directions in parameter space appear to be general properties of shrimp-shaped structures (see [14]). These structures are abundant in the parameter space as can be seen by the magnification shown in Figs. 3(c)-(d). As the parameter space is searched further and further for finer domains, a large amount of distinct ISSs appear, usually well organized and sometimes even connected to each other [see the connected shrimp-shaped ISSs in Fig. 3(c)]. Connected shrimps have the same current value. Although almost all ISSs present finite  $\mathcal{RC}$ s, some ISSs present zero currents inside. We mention one

example which can nicely be observed in Fig. 3(a) close to  $K = 4.5$  and  $\gamma = 0.75$  [compare with the cyan ISS from Fig. 3(b)]. Such very interesting cases will be analyzed in another work.

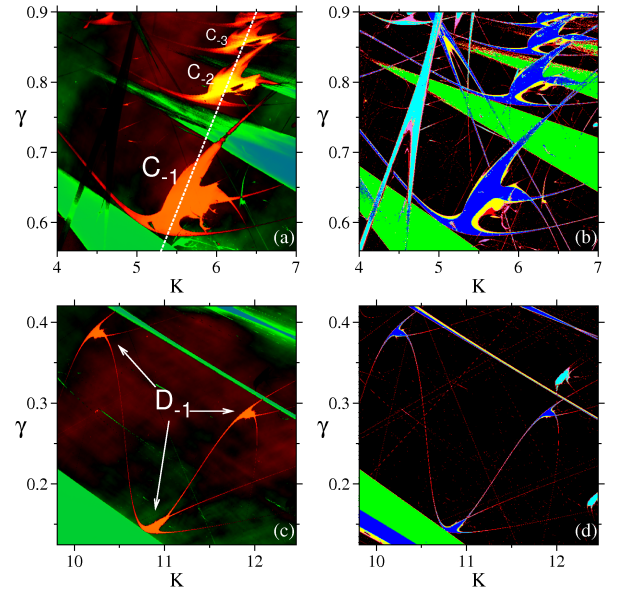


Figure 3. (Color online) Magnifications of Fig. 1 (left) and Fig. 2 (right) showing that the ISSs are abundant inside the chaotic region and usually organized along specific lines and sometimes connected to each other.

The region  $E$  presents larger currents close to  $\gamma = 1$  with not well defined borders. We start by mention that the parameter space for the largest LE (not shown here) in this region is positive and thus totally chaotic. We also clearly see from Figs. 1 and 2 that ISSs with larger  $L$  start to overlap to each other when  $\gamma \rightarrow 1$  and thus the number of stable periodic points in phase space increases more and more. But the interesting point is that apparently the periodic structures are not directly responsible for the currents in region  $E$ . For one example see the preferential line along the structures  $C_{-1}, C_{-2} \dots$  in Fig. 3(a), where the currents increase negatively as  $\gamma \rightarrow 1$ . If the  $C_L$  structures were responsible for the current in  $E$ , we would expect a very large negative current. However, this is not what happens since a current reversal occurs close to  $\gamma \rightarrow 1$  (see green region in Fig. 1 at the end of the  $C_{-1}, C_{-2} \dots$  sequence). In fact, close to  $\gamma = 1$  we have regions of multistability and chaotic motion were the dynamics, which is a mixture of a large number of periodic and chaotic attractors, each one with his own basin of attraction, is very rich and complex. Such multistability regions were analyzed for the kicked rotor in the beautiful works of [21, 22]. The “competition” between multistable and chaotic attractors in order to generate the  $\mathcal{RC}$  is gained by the larger basin of attractions of chaotic attractors. Extensive numerical simulations show that close to  $\gamma = 1$  the unsharply borders do

not change for larger iteration times and that the basins of attraction of periodic orbits are very small compared to the basins of chaotic attractors. This agrees with some recent works [5, 19, 23, 24] which suggest that the  $\mathcal{RC}$  in this region is due to the mixture of chaotic motion with tiny island from the conservative case. In fact, accelerator modes from  $\gamma = 1$  are responsible for the asymmetry of chaotic attractors, generating the currents.

In order to show that  $\mathcal{RC}$ s present generic ISSs in the parameter space of a more general class of dynamical systems, we analyze the zero temperature Langevin equation:  $\ddot{x} + \gamma\dot{x} - 5.0 [\sin(x) + 0.7 \sin(2x - \frac{\pi}{2})] - K_t \sin(1.0t) = 0$ .  $K_t$  is the amplitude of the external time oscillating force,  $\gamma$  is the viscosity and the force coming from the ratchet potential is identical from Eq. (1). Figure 4 shows the  $\mathcal{RC}$  in a smaller portion of the pa-

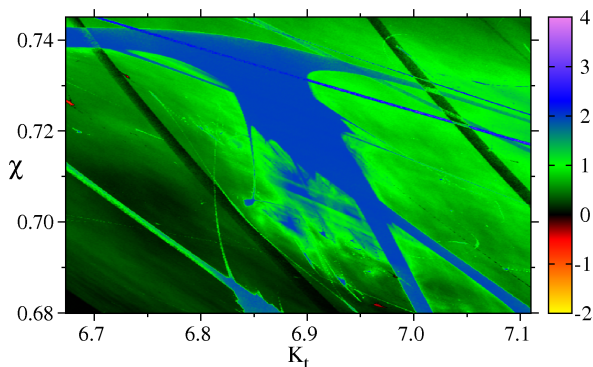


Figure 4. (Color online) Current in the parameter space ( $K_t, \chi = e^{(-\gamma)}$ ) for the Langevin equation.

parameter space ( $K_t, \chi = e^{(-\gamma)}$ ). As in Fig. 1, larger currents can be observed in the large blue shrimp-shaped ISS with main period  $q = 2$ . Again doubling bifurcations occur inside the ISS (not shown), as observed in Figs. 2 and 3(d) for the  $D_{-1}$  and  $D_{-1/2}$  ISSs. Behind the main shrimp-shaped ISS, a cloudy background is observed and also a large amount of smaller ISSs, which can be better resolved when the parameter space is searched for finer and finer domains. Small finite temperatures will slowly transform the sharp borders of the ISSs into unsharply borders and simultaneously enlarge them since their attractors are more stable under noise effects than the chaotic attractors [25].

Concluding, universal ISSs in parameter space are shown to generate large  $\mathcal{RC}$ s and to organize themselves along preferential directions, which allows to make predictions of the  $\mathcal{RC}$ s along the such directions. Inside a given structure,  $\mathcal{RC}$ s are independent of the period of the orbit. The essential property to obtain finite  $\mathcal{RC}$ s is the momentum asymmetry of attractors in phase space times the size of the corresponding basin of attraction and can be expressed as  $\mathcal{RC} = \sum_{i=1}^{N_a} \langle p \rangle_i S_i$ , where  $N_a$  is the num-

ber of attractors,  $\langle p \rangle_i$  is the mean momentum of attractor  $i$  and  $S_i$  is the size (normalized) of attractor  $i$ . Thus Figs. 1 and 4 are a *direct quantitative measure* of  $\mathcal{RC}$ s. We stress that the isoperiodic stable transport structures  $B_L$  (cuspidal-shaped),  $D_L$  (shrimp-shaped) and  $C_L$  are universal patterns which should appear in the parameter space of any dissipative ratchet system, independent of its application in nature. This was ratified by showing the appearance of the shrimp-shaped ISSs in the parameter space of the Langevin equation with an external unbiased field. It would be very likely to observe the  $\mathcal{RC}$ s ISSs in real experiments.

- 
- [1] L.Cavallasca, R.Artuso, and G.Casati, Phys.Rev.E **75**, 066213 (2007).
  - [2] R.D.Astumian and P.Hänggi, Phys.Today **55**, 33 (2002).
  - [3] P.Reimann, Phys.Rep. **361**, 57 (2002).
  - [4] F.Jülicher, A.Ajdari, and J.Prost, Rev.Mod.Phys. **1997**, 1269 (1997).
  - [5] G.G.Carlo, G.Benenti, G.Casati, and D.L.Shepelyansky, Phys.Rev.Lett. **94**, 164101 (2005).
  - [6] G.Lambert, D.Liao, R.H.Austin, and H.Robert, Phys.Rev.Lett. **104**, 168102 (2010).
  - [7] G.Mahmud et al., Nature Physics **5**, 606 (2009).
  - [8] P.Eshuis, K. der Weele, D.Lohse, and D. der Meer, Phys.Rev.Lett. **104**, 248001 (2010).
  - [9] K.John, P.Hänggi, and U.Thiele, Soft Matter **4**, 1183 (2008).
  - [10] S.Kohler, J.Lehmann, and P.Hänggi, Phys.Rep. **406**, 379 (2005).
  - [11] J.B.Gong and P.Brumer, Ann.Rev.Phys.Chem. **56**, 1 (2005).
  - [12] J.Lehmann, S.Kohler, V.May, and P.Hänggi, J.Chem.Phys. **121**, 2278 (2004).
  - [13] T. Dittrich and N. Naranjo, Chem.Phys. **375**, 486 (2010).
  - [14] J.A.C.Gallas, Phys.Rev.Lett. **70**, 2714 (1993).
  - [15] S.Hayes, C.Grebogi, and E.Ott, Phys.Rev.Lett. **70**, 3031 (1993).
  - [16] M. S. Baptista and I. L. Caldas, Chaos, Solitons & Fractals **7**, 325 (1996).
  - [17] C.Bonatto and J.A.C.Gallas, Phys.Rev.E **75**, R055204 (2007).
  - [18] R.Stoop, P.Benner, and Y.Uwate, Phys.Rev.Lett. **105**, 074102 (2010).
  - [19] L. Wang, G. Benenti, G. Casati, and B. Li, Phys.Rev.Lett. **99**, 244101 (2007).
  - [20] A. Endler and J.A.C. Gallas, C.R.Acad.Sci.Paris, Ser.I **342**, 681 (2006).
  - [21] L.C. Martins and J.A.C. Gallas, Int.J.Bif.Chaos **18**, 1705 (2008).
  - [22] U.Feudel, C.Grebogi, B.R.Hunt, and J.A.Yorke, Phys.Rev.E **54**, 71 (1996).
  - [23] S.Denisov et al, Phys.Rev.E **66**, 041104 (2002).
  - [24] H. Schanz, M.-F. Otto, R. Ketzmerick, and T. Dittrich, Phys. Rev. Lett. **87**, 070601 (2001).
  - [25] J.A.Blackburn, H.J.T.Smith, and N.Gronbeh-Jensen, Phys.Rev.B **53**, 14546 (1996).